The Astronomical Journal, 155:251 (8pp), 2018 June https://doi.org/10.3847/1538-3881/aac172

The Origin of Titan's External Oxygen: Further Constraints from ALMA Upper Limits on CS and CH_2NH

N. A. Teanby[1], M. A. Cordiner[2], C. A. Nixon[2], P. G. J. Irwin[3], S. M. Hörst[4], M. Sylvestre[1], J. Serigano[4], A. E. Thelen[5], A. M. S. Richards[6], and S. B. Charnley[2]

[1] School of Earth Sciences, University of Bristol, Wills Memorial Building, Queens Road, Bristol BS8 1RJ, UK; n.teanby@bristol.ac.uk
[2] NASA Goddard Space Flight Center, 8800 Greenbelt Road, Greenbelt, MD 20771, USA
[3] Atmospheric, Oceanic and Planetary Physics, Clarendon Laboratory, University of Oxford, Parks Road, Oxford OX1 3PU, UK
[4] Department of Earth and Planetary Sciences, Johns Hopkins University, Baltimore, MD 21218, USA
[5] Department of Astronomy, New Mexico State University, Las Cruces, NM 88003-8001, USA
[6] Jodrell Bank Centre for Astrophysics, School of Physics and Astronomy, University of Manchester, Manchester, UK
Received 2018 March 9; revised 2018 April 25; accepted 2018 April 27; published 2018 May 25

Abstract

Titan's atmospheric inventory of oxygen compounds (H_2O, CO_2, CO) are thought to result from photochemistry acting on externally supplied oxygen species (O^+, OH, H_2O). These species potentially originate from two main sources: (1) cryogenic plumes from the active moon Enceladus and (2) micrometeoroid ablation. Enceladus is already suspected to be the major O^+ source, which is required for CO creation. However, photochemical models also require H_2O and OH influx to reproduce observed quantities of CO_2 and H_2O. Here, we exploit sulphur as a tracer to investigate the oxygen source because it has very different relative abundances in micrometeorites ($S/O \sim 10^{-2}$) and Enceladus' plumes ($S/O \sim 10^{-5}$). Photochemical models predict most sulphur is converted to CS in the upper atmosphere, so we use Atacama Large Millimeter/submillimeter Array (ALMA) observations at ~340 GHz to search for CS emission. We determined stringent CS 3σ stratospheric upper limits of 0.0074 ppb (uniform above 100 km) and 0.0256 ppb (uniform above 200 km). These upper limits are not quite stringent enough to distinguish between Enceladus and micrometeorite sources at the 3σ level and a contribution from micrometeorites cannot be ruled out, especially if external flux is toward the lower end of current estimates. Only the high-flux micrometeorite source model of Hickson et al. can be rejected at 3σ. We determined a 3σ stratospheric upper limit for CH_2NH of 0.35 ppb, which suggests cosmic rays may have a smaller influence in the lower stratosphere than predicted by some photochemical models. Disk-averaged C_3H_4 and C_2H_5CN profiles were determined and are consistent with previous ALMA and Cassini/CIRS measurements.

Key words: planets and satellites: atmospheres – planets and satellites: individual (Titan) – radiative transfer

1. Introduction

Titan is the largest moon of Saturn and has a thick N_2/CH_4 atmosphere with a diverse chemical inventory including hydrocarbons, nitrogen species, and oxygen compounds. Titan's exotic nitrile and hydrocarbon species are created in situ by photochemical reactions driven by dissociation of CH_4 and N_2 to form radicals (e.g., Lavvas et al. 2008; Loison et al. 2015; Vuitton et al. 2018). However, Titan's oxygen species require an external oxygen source, initially mostly in the form of water, O^+, and OH, which are subsequently modified by photochemistry into three main oxygen-bearing species: CO, CO_2, and H_2O (Hörst et al. 2008; Dobrijevic et al. 2014). The oxygen source must be external in order to explain measurements of water in Titan's stratosphere (Coustenis et al. 1998; Cottini et al. 2012; Moreno et al. 2012); surface or internal sources are not viable because water vapor would be removed by condensation at the tropopause cold trap before ever reaching the stratosphere. This does not rule out additional internal sources of non-condensing CO, so a wide range of sources must still be considered (Dobrijevic et al. 2014).

Despite its importance for understanding Titan's photochemistry and space environment, significant uncertainties remain about oxygen's origin, with the two main candidates being: (1) Enceladus' plumes and (2) micrometeorites. We know there is an O^+ flux into Titan's atmosphere from Cassini/CAPS measurements (Hartle et al. 2006a, 2006b) and the source appears to be Enceladus (Hartle et al. 2006a, 2006b; Hörst et al. 2008; Cassidy & Johnson 2010). This can explain the current observed 50 ppm CO abundance (de Kok et al. 2007; Teanby et al. 2010; Serigano et al. 2016). However, OH and H_2O fluxes are also required to explain Titan's CO_2 and H_2O stratospheric abundances (Hörst et al. 2008; Dobrijevic et al. 2014). An external H_2O flux of approximately 1–3 $\times$ 10^6 cm^{-2} s^{-1} is required based on the observed water abundance (Coustenis et al. 1998; Sittler et al. 2009). Unfortunately, current estimates of the oxygen flux from Enceladus and micrometeorites have large uncertainties, with a wide range of possible values from 0–6 $\times$ 10^6 cm^{-2} s^{-1} being reported for both sources (English et al. 1996; Hartle et al. 2006a, 2006b; Sittler et al. 2009; Cassidy & Johnson 2010). Therefore, observations of the H_2O profile alone do not sufficiently constrain the source. Determining the relative contribution from each source would allow self-consistent photochemical models to be developed. Also, if micrometeorites make a significant contribution we would need to rethink the way oxygen fluxes are treated in photochemical models to allow for a more chemically diverse source. Further observational constraints on Titan's external oxygen fluxes are required to address this uncertainty.

The Atacama Large Millimeter/submillimeter Array (ALMA) has proven to be extremely sensitive to minor species in Titan's atmosphere (e.g., Cordiner et al. 2015; Palmer et al. 2017). However, instead of observing the oxygen species

directly, our approach here is to address the puzzle of Titan's external oxygen supply by observing a tracer species to diagnose the origin. Sulphur species provide an ideal tracer for this application as they have very different abundances in the two candidate source populations: in micrometeorites sulphur species have a total abundance relative to water of $\sim 10^{-2}$ (Crovisier et al. 2009), whereas for Enceladus' plumes the total abundance relative to water is three orders of magnitude lower at $\sim 10^{-5}$ (Waite et al. 2009). Therefore, sulphur provides a sensitive tracer of the external oxygen flux's origin and its abundance could potentially be used to determine the fraction of external flux from each source.

Recent photochemical modeling predicts that in Titan's atmosphere, all three major sulphur species (H_2S, CS, OCS) will be mostly converted into carbon monosulphide CS (Hickson et al. 2014) for altitudes above 200 km. Below 200 km altitude H_2S is expected to be the dominant sulphur reservoir (Hickson et al. 2014). CS has strong isolated molecular emission lines in the submillimeter, so was chosen as our primary observational target. A high CS abundance would indicate a significant micrometeorite contribution for Titan's external flux, whereas a low abundance would indicate that Enceladus's plumes are the primary origin.

An additional goal was to study the role of cosmic rays in the lower stratosphere. Cosmic rays are predicted to cause nitrogen dissociation at altitudes of 100–200 km, which can locally enhance production of nitrogen bearing trace gases (Wilson & Atreya 2004; Lavvas et al. 2008; Loison et al. 2015; Vuitton et al. 2018). One effect of these cosmic rays should be to produce an abundance spike in CH_2NH, which has an emission feature close to our main CS line. Therefore, the abundance of CH_2NH can be used to test cosmic-ray processes in photochemical models.

Our results have implications for understanding Titan's rich photochemistry, atmospheric origins, and general external flux sources in the outer solar system.

2. Observations

ALMA observations were taken under Cycle 4 project 2016.1.00154.S "The origin of Titan's external oxygen" (PI: N. A. Teanby). Two CS lines were targeted: one at 244.936 GHz in Band 6 and a second at 342.883 GHz in Band 7. However, only the Band 7 observations were taken due to scheduling, observational, and weather constraints.

Observations were taken on 2017 March 23 08:07:26 UTC with a total observation time of 35.42 minutes including 8.06 minutes integration on Titan in the most compact C40-1 array configuration (40 antennas with baselines of 15–161 m) giving an approximate spatial resolution of 1″. This integration time gave the maximum possible signal-to-noise ratio, which is limited by ALMA's maximum spectral dynamic range of 500 in Band 7. Band 6 has a higher dynamic range of 1000, but the CS spectral features are about half as intense, so would have resulted in a comparable signal to noise. Therefore, we estimate a factor of $\sqrt{2}$ reduction in signal to noise was caused by the loss of the Band 6 observations. Titan was also used as the flux calibrator, which introduces an uncertainty on the absolute flux of ≈15%. Two 1875 MHz bandwidth spectral windows (SPW) were observed with central frequencies of 340.6375 GHz (SPW0) and 342.4125 GHz (SPW1) to cover emission lines of CS, CH_2NH, C_3H_4, and C_2H_5CN. The raw channel spacing was 0.488 MHz, with a factor of two smoothing applied during acquisition to give a recorded channel spacing of 0.977 MHz and a spectral resolution FWHM of 1.129 MHz.

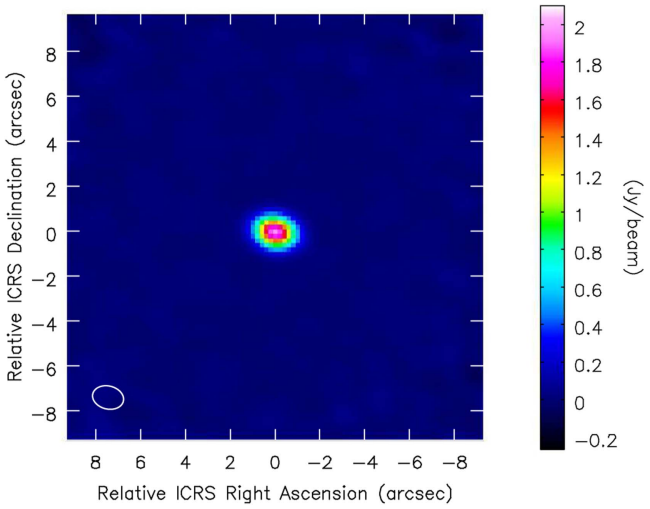

Figure 1. ALMA emission map of Titan. The map is plotted at the central frequency of SPW0 (340.6375 GHz). White ellipse indicates synthesized beam (1.3 × 0.″95), which is larger than Titan's solid body diameter of 0.″716, so Titan is not resolved. Image has been deconvolved using the `clean` algorithm and corrected for the primary beam response using `pbcor` in CASA.

The data were reduced using CASA pipeline version 4.7.2 (McMullin et al. 2007) using the standard data reduction pipeline scripts supplied with the observation. Imaging was carried out using the `clean` algorithm with a threshold of twice the rms noise, 0.2 × 0.″2 pixels, and a 128 × 128 image size for the deconvolution. This resulted in a 1.3 × 0.″95 synthesized beam and an rms noise of ≈7 mJy/beam. Titan was at a distance of 9.92 au during the observations, resulting in a solid body diameter of 0.″716 and disk-averaged spectra. Radiances were corrected for the primary beam response using the `impbcor` task and output into FITS format using `exportfits` for further analysis. The cleaned image is shown in Figure 1.

To obtain an overall disk-averaged spectrum of Titan from the cleaned images the radiance was integrated over a 7 pixel (1.″4) radius circle centered on Titan for spectral windows SPW0 and SPW1, which gave the total disk-average irradiance in Janskys. These spectra were shifted in frequency to account for a blueshift of 33.2 km s^{-1}, calculated using JPL-Horizons, to map them into Titan's rest frame. The frequency scale and continuum level of these spectra were verified against a Titan reference spectrum based on Cassini observations (described in Teanby et al. 2013). Cross correlation with the reference showed the residual frequency shift was less than a spectral resolution element, so no further frequency correction was required. However, the continuum level of the spectra needed to be multiplied by a factor of 1.085 to bring them into agreement with the reference spectrum—this is comparable to the absolute flux uncertainty limits of the ALMA pipeline. Finally, SPW0 and SPW1 were combined into a single spectrum (Figure 2(a)). The final spectrum shows obvious emission features from C_3H_4 and C_2H_5CN, but CS and CH_2NH emission lines are not apparent.

3. Radiative Transfer Model

Spectra were analyzed with the NEMESIS radiative transfer retrieval code (Irwin et al. 2008), which we have previously

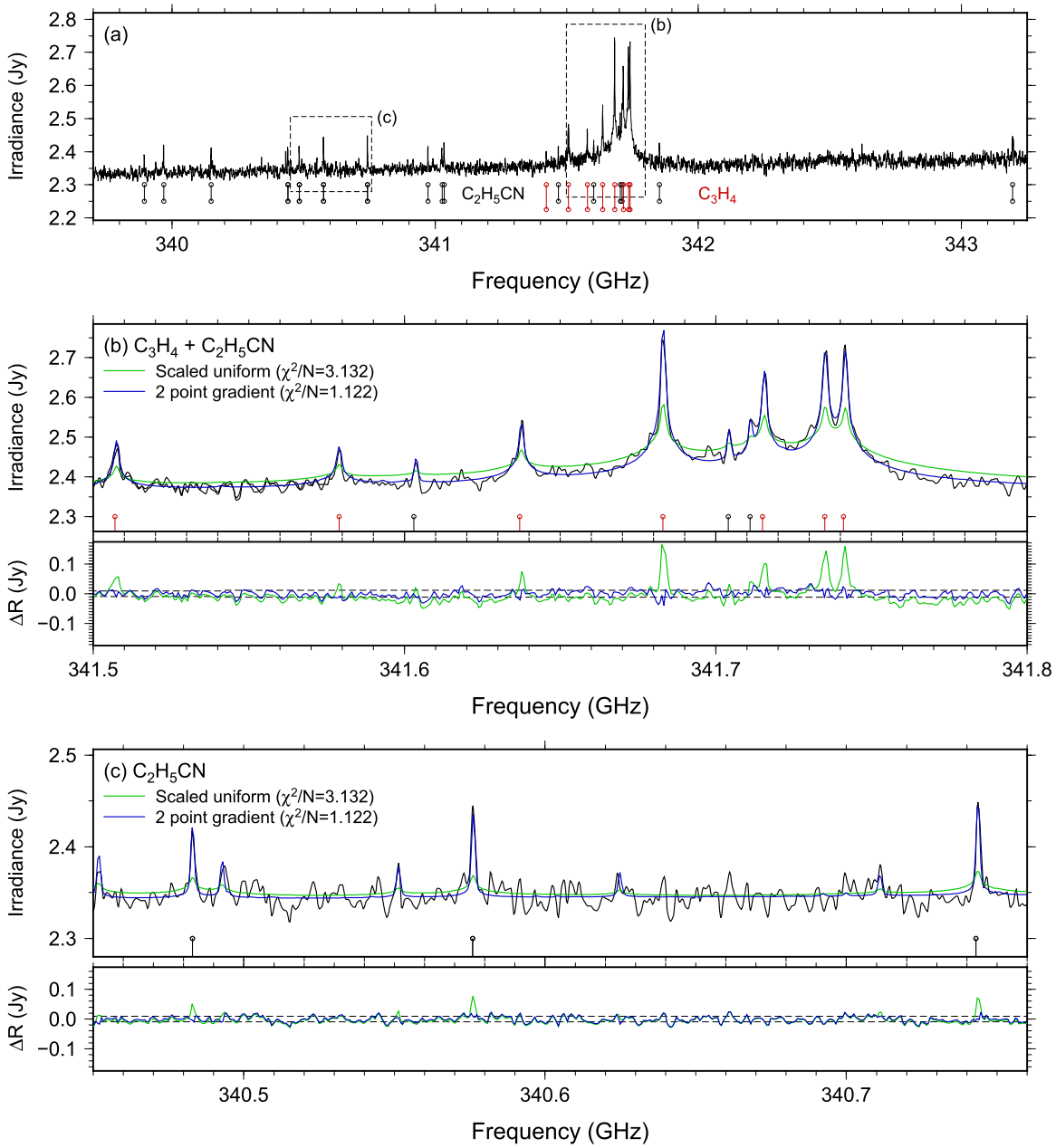

Figure 2. Observed disk-averaged ALMA Titan spectrum. (a) Combined spectrum from SPW0 and SPW1. Irradiances have been calculated by integrating the emission over a 1.″4 radius Titan-centric circular area of the observation plotted in Figure 1. Black/red vertical ticks indicate C_2H_5CN/C_3H_4 spectral features, respectively. The overall rms noise level is 12 mJy. ((b), (c)) Fits to the measured spectra using uniform and two-point gradient vertical profiles for C_2H_5CN and C_3H_4 (shown in Figure 3). Subplots show the difference (ΔR) between observed and fitted irradiance, with dashed lines indicating the rms noise level.

applied to analysis of Titan submillimeter spectra from ALMA (Cordiner et al. 2015; Serigano et al. 2016; Palmer et al. 2017) and Herschel/SPIRE (Teanby et al. 2013). The modeling approach follows that discussed in detail in Teanby et al. (2013).

The reference atmospheric composition and temperature profile (Figure 3(d)) are based on analysis of Cassini/Huygens data and are fully defined in Teanby et al. (2013). Spectroscopic parameters are also the same as those used in Teanby et al. (2013), except that additional submillimeter transitions were included from the JPL (C_3H_4, CS, CH_2NH) and CDMS (C_2H_5CN) spectral databases. For C_3H_4 lines we used a Lorentzian half-width of $\Gamma = 0.1$ cm^{-1} at 296 K with a temperature dependence exponent of $n = 0.75$ following Vinatier et al. (2007). For CS, CH_2NH, and C_2H_5CN we assumed $\Gamma = 0.075$ cm^{-1} and $n = 0.5$ as in Cordiner et al. (2015). To improve computational efficiency, spectra were modeled using the correlated-k approximation (Goody & Yung 1989; Lacis & Oinas 1991) and the 1.129 MHz FWHM instrument function was incorporated directly into the k-tables.

To accurately reproduce Titan's disk-averaged spectrum we followed the approach of Teanby et al. (2013), where synthetic spectra are generated using an area-weighted average of multiple viewing geometries. For this study we used 60 viewing geometries: 10 covering Titan's disk and 50 off the limb to cover Titan's extended atmosphere up to a maximum altitude of 1250 km, above which the modeled radiance became negligible.

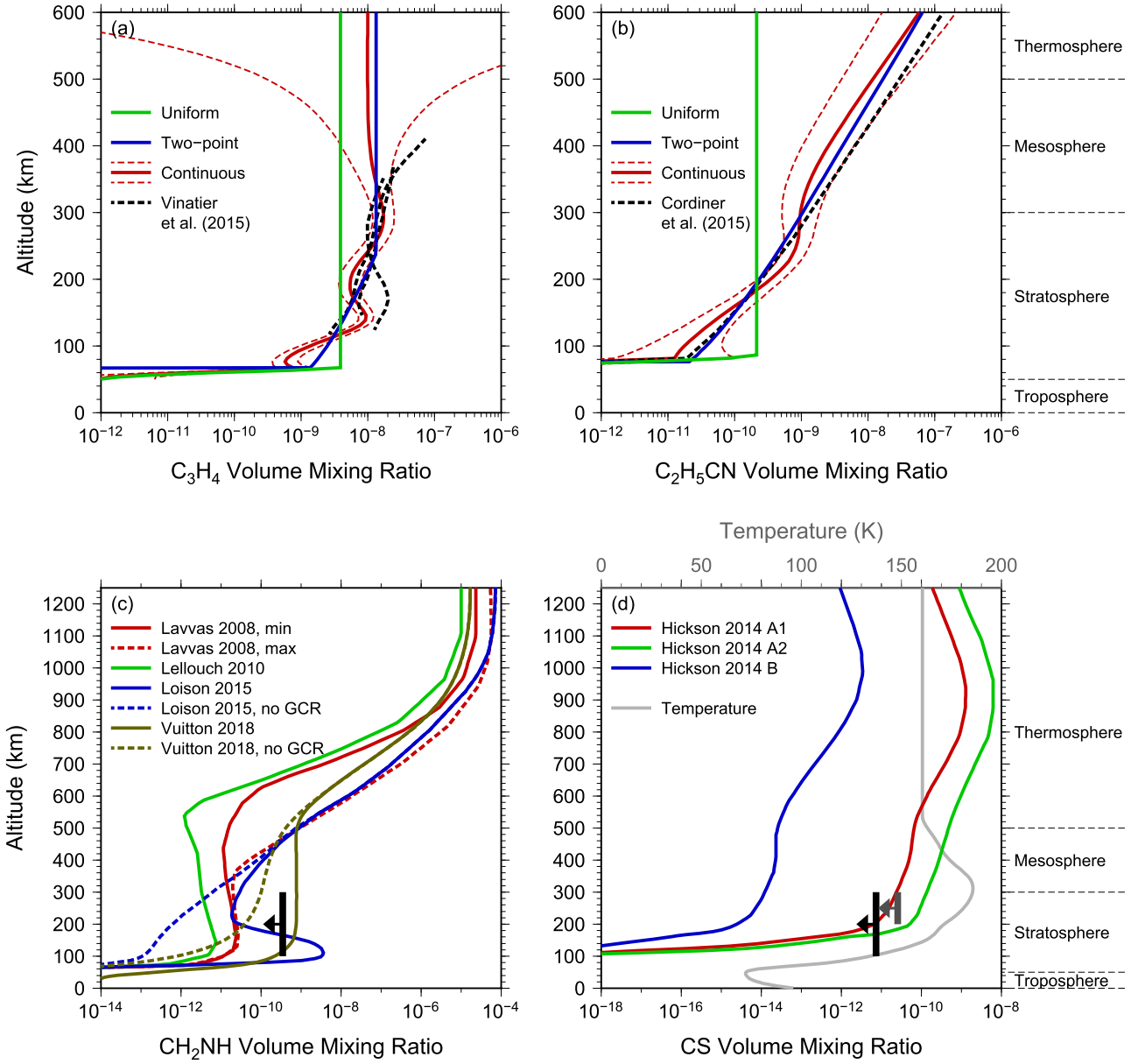

Figure 3. Volume mixing ratio profiles. (a) C_3H_4 and (b) C_2H_5CN profiles retrieved from the observed spectrum in Figure 2 using NEMESIS (Irwin et al. 2008). The two-point gradient profiles were constructed to be a simplified version of the continuously retrieved profiles and were found to fit the spectrum to within errors. Our C_3H_4 profile is consistent with equatorial and mid-latitude profiles from Cassini/CIRS (Vinatier et al. 2015) and our C_2H_5CN profile is consistent with previous disk-averaged results from ALMA at 220–240 GHz (Cordiner et al. 2015). ((c), (d)) Photochemical model profiles for CH_2NH and CS from Lavvas et al. (2008), Lellouch et al. (2010), Hickson et al. (2014), Loison et al. (2015), and Vuitton et al. (2018), which were used to determine upper limit scale factors (Table 1). Our 3σ upper limits for uniform profiles are indicated with black vertical bars. Gray vertical bar shows the CS upper limit for a uniform profile with a photochemical sink cutoff below 200 km. The atmospheric temperature profile is also shown in (d).

Gas emission lines of C_3H_4 and C_2H_5CN were fitted using three methods: (1) scaling a volume mixing ratio profile that was uniform above the condensation level; (2) inverting for a continuous profile with a correlation length of one atmospheric scale height to give a smooth profile; and (3) retrieving a simple linear gradient model defined by two points, with a constant abundance above the highest point and zero abundance below the lower point. The lower altitude points were chosen to match the condensation level, whereas the upper level was chosen based on an inspection of the continuous profiles (300 km for C_3H_4 and 600 km for C_2H_5CN). Condensation was calculated using the vapor pressure data in Haynes (2011) and the temperature profile shown in Figure 3(d).

For gases that did not show obvious emission features in the observed spectrum, we instead calculate upper limits using the χ^2 statistic defined by

$$\chi^2 = \frac{\Delta\nu_{\rm obs}}{\Delta\nu_{\rm res}} \sum_{i=1}^{N} \left[\frac{f(\nu_i, v_i) - y(\nu_i)}{\sigma(\nu_i)} \right]^2, \quad (1)$$

where $y(\nu_i)$ is the observed spectrum at frequency ν_i, $f(\nu_i, v_i)$ is the synthetic spectrum for a gas volume mixing ratio of v_i, $\sigma(\nu_i)$ is the rms observation error per channel, N is the number of observed frequencies considered, $\Delta\nu_{\rm obs}$ is the frequency spacing of the observations (0.977 MHz), and $\Delta\nu_{\rm res}$ is the spectral resolution (1.129 MHz). Synthetic spectra were generated with profiles that were uniform above the condensation level or by

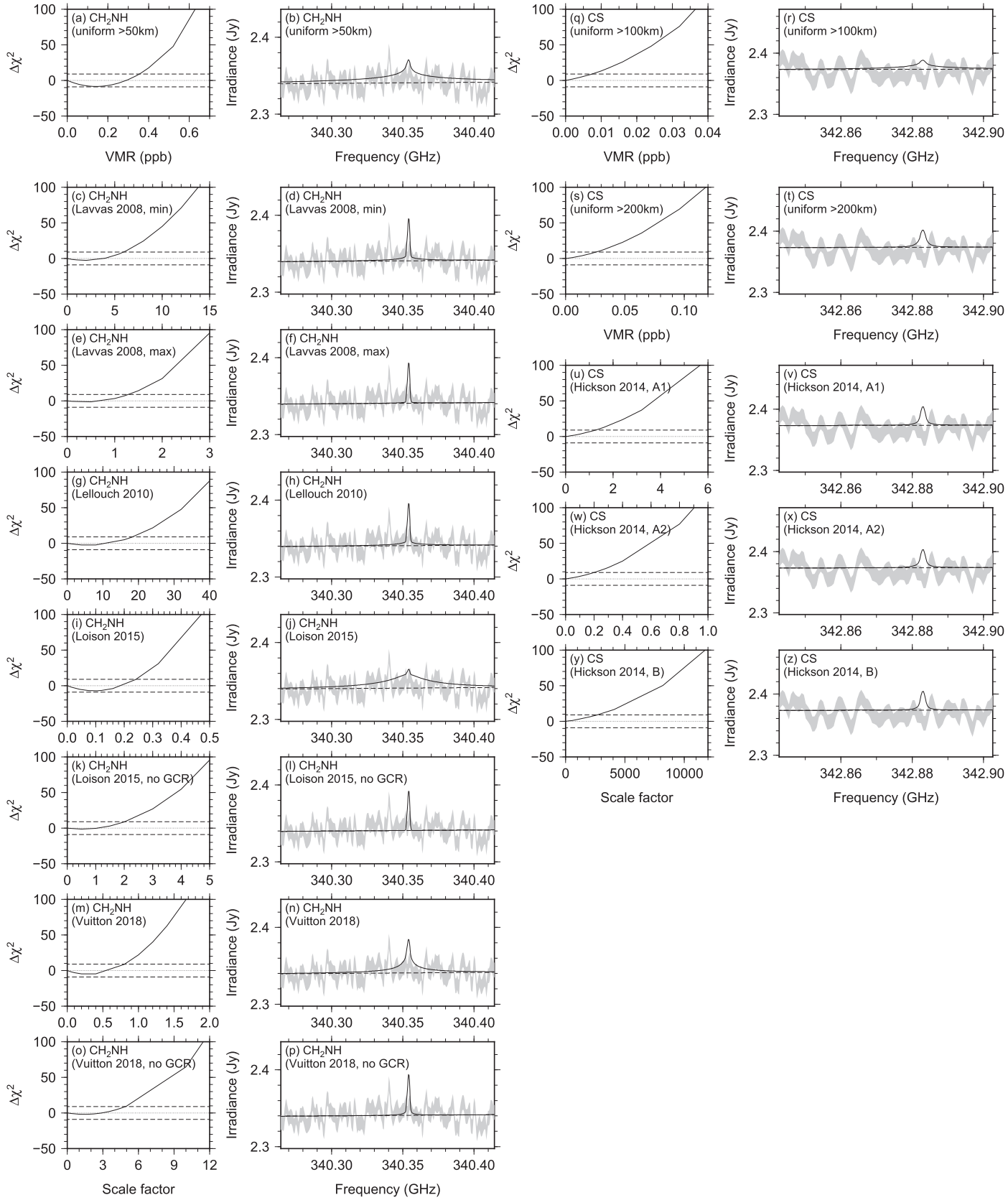

Figure 4. Upper limit calculations for (a)–(p) CH_2NH and (q)–(z) CS. Left panels in each column show the increase in misfit ($\Delta\chi^2$) as a function of either volume mixing ratio (for uniform profiles) or scale factor (for photochemical profiles). Right panels in each column show the measured spectrum (gray) with a synthetic spectrum corresponding to the 3σ upper limit. The upper limits are summarized in Table 1.

Table 1
Upper Limits of CS and CH_2NH

Gas	Frequency (GHz)	Profile	Upper limits: VMR† 3σ	Scale factor 3σ	Scale factor 2σ	Reject Profile 3σ	Reject Profile 2σ
CS	342.883	Uniform >100 km	<0.0074 ppb	…	…	…	…
CS	342.883	Uniform >200 km	<0.0256 ppb	…	…	…	…
CS	342.883	Hickson et al. (2014) (A1)	…	<1.25	<0.68	N	Y
CS	342.883	Hickson et al. (2014) (A2)	…	<0.20	<0.11	Y	Y
CS	342.883	Hickson et al. (2014) (B)	…	<2665	<1415	N	N
CH_2NH	340.354	Uniform >50 km	<0.35 ppb	…	…	…	…
CH_2NH	340.354	Lavvas et al. (2008) (min)	…	<5.93	<4.89	N	N
CH_2NH	340.354	Lavvas et al. (2008) (max)	…	<1.29	<1.04	N	N
CH_2NH	340.354	Lellouch et al. (2010)	…	<18.3	<15.0	N	N
CH_2NH	340.354	Loison et al. (2015)	…	<0.24	<0.17	Y	Y
CH_2NH	340.354	Loison et al. (2015) (no GCR)	…	<2.01	<1.58	N	N
CH_2NH	340.354	Vuitton et al. (2018)	…	<0.80	<0.52	Y	Y
CH_2NH	340.354	Vuitton et al. (2018) (no GCR)	…	<4.88	<3.97	N	N

Note. Upper limits refer either to a volume mixing ratio (VMR) above the condensation level for uniform profiles or a scale factor applied to the referenced photochemical profile. If the $3\sigma/2\sigma$ upper limit scale factor for a given profile is <1, then the profile is not consistent with the observations at the $3\sigma/2\sigma$ level. †ppb is parts per billion by volume.

scaling photochemical model profiles from Lavvas et al. (2008), Lellouch et al. (2010), Hickson et al. (2014), Loison et al. (2015), and Vuitton et al. (2018) (Figure 3). For the uniform profiles, condensation was assumed to occur at 100 km for CS and 50 km for CH_2NH. These exact levels are not critical for the analysis as the contribution functions for uniform profiles peak in the stratosphere in the range 100–300 km. However, for CS we also used a profile that was uniform above 200 km altitude, in an attempt to represent photochemical processes that convert CS into H_2S below 200 km (Hickson et al. 2014).

4. Results

The fits to the measured C_3H_4 and C_2H_5CN spectral features are shown in Figures 2(b) and (c). Scaling uniform (above the condensation level) volume mixing ratio profiles does not fit the observations sufficiently well within the uncertainties and results in a χ^2/N of 3.13. It is apparent that this profile results in extended line wings that are not supported by the data. The two-point gradient profile fits the observations very well ($\chi^2/N = 1.12$) and the continuous profile provides only a slight improvement ($\chi^2/N = 1.04$, synthetic spectra not plotted). Therefore, the extra complexity of the continuous profile cannot be justified by these data alone and the two-point profiles are preferred. Figure 3 also compares our retrieved volume mixing ratio profiles to previous results from Cassini/CIRS (C_3H_4; Vinatier et al. 2015) and ALMA (C_2H_5CN; Cordiner et al. 2015), which are consistent with our results.

Figure 4 shows a χ^2 analysis of uniform and photochemical profiles for CS and CH_2NH. For a 3σ detection of CS or CH_2NH the change in χ^2 should be -9 or less (Press et al. 1992). This is not the case for these spectra for any of the profiles, so we are confined to determining upper limits of these gases. In this case, an increase in χ^2 by $+9/+4$ corresponds to the $3\sigma/2\sigma$ upper limit, which are summarized in Table 1. For a vmr profile that is uniform above the condensation level the 3σ upper limits are 0.35 ppb for CH_2NH, 0.0074 ppb for CS (uniform above 100 km), and 0.0256 ppb for CS (uniform above 200 km). These upper limits are most appropriate for the stratosphere (100–300 km) and are indicated in Figure 3.

5. Discussion

The primary aim of this study is to provide constraints on Titan's external oxygen source using CS as a tracer, which we can now address using our upper limits.

Hickson et al. (2014) consider three external source scenarios: (1) A1, micrometeorite source with external fluxes of 5.2×10^5 cm^{-2} s^{-1} for H_2O and 1.6×10^6 cm^{-2} s^{-1} for O, which has an H_2O flux consistent with the Herschel/PACS water vapor measurements by Moreno et al. (2012); (2) A2, micrometeorite source with external fluxes of 2.6×10^6 cm^{-2} s^{-1} for H_2O and zero for O, which has a ~4 times greater H_2O flux consistent with the Cassini/CIRS water vapor measurement by Cottini et al. (2012); and (3) B, Enceladus source with external fluxes of 6.5×10^5 cm^{-2} s^{-1} for H_2O, and 1.6×10^6 cm^{-2} s^{-1} for O. For the micrometeorite sources (A1, A2) the abundance of sulphur species relative to H_2O was assumed to be 1.5×10^{-2} for H_2S, 4×10^{-3} for OCS, and 2×10^{-3} for CS. For the Enceladus source (B) the abundance of H_2S relative to H_2O was assumed to be 10^{-5} with zero OCS and CS flux.

Based on the upper limits in Table 1, scenarios A1 and B are consistent with our observations, but scenario A2 with the higher H_2O flux is not consistent and can be rejected. Therefore, if the model of Hickson et al. (2014) is correct, this implies that the lower H_2O flux inferred from Herschel/PACS (Moreno et al. 2012) is more consistent with our upper limits than the higher flux implied by Cottini et al. (2012). Bauduin et al. (2018) investigate whether the discrepancy between Herschel/PACS and Cassini/CIRS determinations could be due to different analysis techniques by re-analyzing both data sets using a common retrieval scheme. They conclude that the difference is real, which raises the question of latitude and temporal variations in H_2O flux. Therefore, the steady state fluxes assumed by the model may not be entirely appropriate.

Unfortunately, due to the loss of our Band 6 observations, the upper limit for CS is not quite stringent enough to distinguish between an Enceladus and micrometeorite source at the 3σ level, although a solely micrometeorite source can still be rejected at the 2σ level. This is consistent with the observations of O^+ into Titan's atmosphere from Cassini/CAPS (Hartle et al. 2006a, 2006b) and the inference of an Enceladus source for these ions (Hartle et al. 2006a, 2006b; Hörst et al. 2008; Cassidy & Johnson 2010).

In addition, our observations provide the most stringent upper limit so far for CH_2NH: 0.35 ppb in the stratosphere. This can be combined with the CASSINI/INMS detection of 10^{-5} at 1100 km altitude (Vuitton et al. 2007) to constrain the vertical profile. Our results imply a steep vertical gradient, consistent with the profiles presented by Lavvas et al. (2008), Lellouch et al. (2010), Loison et al. (2015), and Vuitton et al. (2018). The only photochemical model profiles that are not entirely consistent with our observations are the profiles with active galactic cosmic rays (GCRs) from Loison et al. (2015) and Vuitton et al. (2018). GCRs result in additional nitrogen photolysis in the lower stratosphere, which leads to increased CH_2NH abundances. In particular, the Loison et al. (2015) profile has ~3 ppb CH_2NH at 100–200 km. This high an abundance would have been easily detectable by our observations. However, comparing Cassini/CIRS observations (Teanby et al. 2009) to photochemical models (Wilson & Atreya 2004) suggests that at least some GCR dissociation of N_2 must occur in the lower stratosphere in order to explain the observed equatorial abundance of C_2N_2. Taking these findings together suggests that GCRs do have an effect on Titan's photochemistry, but at a reduced level compared to current model predictions.

In this study, we focused on CS, which is predicted to be the dominant sulphur species above 200 km (Hickson et al. 2014), but other sulphur species such as H_2S may be present in Titan's atmosphere. Cryovolcanism has also been considered and could potentially release sulphur in the form of ammonium sulphate into the troposphere (Fortes et al. 2007), although any sulphur in the form of H_2S would be limited to sub parts per trillion levels in the stratosphere due to condensation at the tropopause cold trap. H_2S has a current upper limit of 330 ppb in the stratosphere (Nixon et al. 2013) that does not further constrain the oxygen source.

6. Conclusion

We used ALMA observations of Titan at ~340 GHz to determine a new upper limit of 0.0074 ppb for CS in the stratosphere assuming a uniform profile above a 100 km altitude condensation level, or 0.0256 ppb for a profile that is uniform above a 200 km photochemical sink level. We also calculated upper limit scale factors for photochemical model profiles predicted by Hickson et al. (2014). The upper limits allow us to constrain the origin of external oxygen into Titan's atmosphere based on the S/O ratio in the two main source candidates: Enceladus and micrometeorites. The observations are most consistent with an Enceladus source for Titan's external oxygen, and we are able to reject a solely micrometeorite source at the 2σ or 3σ level for low (Moreno et al. 2012) and high (Cottini et al. 2012) external fluxes, respectively. However, a mixture of sources cannot be ruled out with these data, especially given uncertainties in the photochemical schemes. Modest improvements to these upper limits would be possible with observations of additional CS spectral features. However, as the observations were taken at limit of ALMA's dynamic range, such improvements would only scale as the square root of the number of features observed.

A 3σ upper limit for stratospheric CH_2NH of 0.35 ppb was also obtained (assuming a uniform profile above a 50 km altitude condensation level). Comparing this value to the Cassini/INMS measurement of 10^{-5} at 1100 km altitude (Vuitton et al. 2007) shows that CH_2NH has a steep vertical profile and short atmospheric lifetime consistent with photochemical model predictions (Lavvas et al. 2008; Lellouch et al. 2010; Loison et al. 2015; Vuitton et al. 2018). An inconsistency with the GCR-driven profiles of Loison et al. (2015) and Vuitton et al. (2018) suggest that GCR influence on the nitrogen chemistry is less than predicted. All other photochemical profiles we tested, including Loison et al.'s (2015) and Vuitton et al.'s (2018) profiles without GCRs, were consistent with the observations.

Finally, emission features of C_3H_4 and C_2H_5CN were observed, which allowed limited vertical profile information to be retrieved. The retrieved profile gradients were consistent with previous ALMA (Cordiner et al. 2015) and Cassini/CIRS results (Vinatier et al. 2015).

N.A.T., P.G.J.I., and M.S. were funded by the UK Science and Technology Facilities Council. C.A.N. and S.B.C. were supported for their portion of this research by a NASA Science Innovation Fund 2017 Award. A.E.T. was supported by NASA's Office of Education Minority University Research and Education Project AS&ASTAR-JGFP grant No. NNX15AU59. This paper makes use of the following ALMA data: ADS/JAO. ALMA#2016.1.00154.S. ALMA is a partnership of ESO (representing its member states), NSF (USA) and NINS (Japan), together with NRC (Canada), NSC and ASIAA (Taiwan), and KASI (Republic of Korea), in cooperation with the Republic of Chile. The Joint ALMA Observatory is operated by ESO, AUI/NRAO and NAOJ. The National Radio Astronomy Observatory is a facility of the National Science Foundation operated under cooperative agreement by Associated Universities, Inc.

Facility: ALMA.

Software: CASA (McMullin et al. 2007), GMT (Wessel & Smith 1998; Wessel et al. 2013).

ORCID iDs

N. A. Teanby https://orcid.org/0000-0003-3108-5775
S. M. Hörst https://orcid.org/0000-0003-4596-0702

References

Bauduin, S., Irwin, P. G. J., Lellouch, E., et al. 2018, Icar, 311, 288
Cassidy, T. A., & Johnson, R. E. 2010, Icar, 209, 696
Cordiner, M. A., Palmer, M. Y., Nixon, C. A., et al. 2015, ApJL, 800, L14
Cottini, V., Nixon, C. A., Jennings, D. E., et al. 2012, Icar, 220, 855
Coustenis, A., Salama, A., Lellouch, E., et al. 1998, A&A, 336, L85
Crovisier, J., Biver, N., Bockelée-Morvan, D., et al. 2009, EM&P, 105, 267
de Kok, R., Irwin, P. G. J., Teanby, N. A., et al. 2007, Icar, 186, 354
Dobrijevic, M., Hébrard, E., Loison, J. C., & Hickson, K. M. 2014, Icar, 228, 324
English, M. A., Lara, L. M., Lorenz, R. D., Ratcliff, P. R., & Rodrigo, R. 1996, AdSpR, 17, 157
Fortes, A. D., Grindrod, P. M., Trickett, S. K., & Vočadlo, L. 2007, Icar, 188, 139
Goody, R. M., & Yung, Y. L. 1989, Atmospheric Radiation: Theoretical Basis (2nd ed.; Oxford: Oxford Univ. Press)
Hartle, R. E., Sittler, E. C., Neubauer, F. M., et al. 2006a, GeoRL, 33, L08201

Hartle, R. E., Sittler, E. C., Neubauer, F. M., et al. 2006b, P&SS, 54, 1211
Haynes, W. M. (ed.) 2011, CRC Handbook of Chemistry and Physics (92nd ed.; London: Taylor and Francis)
Hickson, K. M., Loison, J. C., Cavalié, T., Hébrard, E., & Dobrijevic, M. 2014, A&A, 572, A58
Hörst, S. M., Vuitton, V., & Yelle, R. V. 2008, JGR, 113, E10006
Irwin, P., Teanby, N., de Kok, R., et al. 2008, JQSRT, 109, 1136
Lacis, A. A., & Oinas, V. 1991, JGR, 96, 9027
Lavvas, P. P., Coustenis, A., & Vardavas, I. M. 2008, P&SS, 56, 67
Lellouch, E., Vinatier, S., Moreno, R., et al. 2010, P&SS, 58, 1724
Loison, J. C., Hébrard, E., Dobrijevic, M., et al. 2015, Icar, 247, 218
McMullin, J. P., Waters, B., Schiebel, D., Young, W., & Golap, K. 2007, in ASP Conf. Ser. 376, Astronomical Data Analysis Software and Systems XVI, ed. R. A. Shaw, F. Hill, & D. J. Bell (San Francisco, CA: ASP), 127
Moreno, R., Lellouch, E., Lara, L. M., et al. 2012, Icar, 221, 753
Nixon, C. A., Teanby, N. A., Irwin, P. G. J., & Hörst, S. M. 2013, Icar, 224, 253
Palmer, M. Y., Cordiner, M. A., Nixon, C. A., et al. 2017, SciA, 3, e1700022
Press, W. H., Flannery, B. P., Teukolsky, S. A., & Vetterling, W. T. 1992, Numerical Recipes (2nd ed.; Cambridge: Cambridge Univ. Press)
Serigano, J., Nixon, C. A., Cordiner, M. A., et al. 2016, ApJL, 821, L8
Sittler, E. C., Ali, A., Cooper, J. F., et al. 2009, P&SS, 57, 1547
Teanby, N. A., Irwin, P. G. J., de Kok, R., et al. 2009, Icar, 202, 620
Teanby, N. A., Irwin, P. G. J., de Kok, R., & Nixon, C. A. 2010, FaDi, 147, 51
Teanby, N. A., Irwin, P. G. J., Nixon, C. A., et al. 2013, P&SS, 75, 136
Vinatier, S., Bézard, B., Fouchet, T., et al. 2007, Icar, 188, 120
Vinatier, S., Bézard, B., Lebonnois, S., et al. 2015, Icar, 250, 95
Vuitton, V., Yelle, R. V., Klippenstein, S. J., Hörst, S. M., & Lavvas, P. 2018, Icar, submitted
Vuitton, V., Yelle, R. V., & McEwan, M. J. 2007, Icar, 191, 722
Waite, J. H., Jr., Lewis, W. S., Magee, B. A., et al. 2009, Natur, 460, 487
Wessel, P., & Smith, W. H. F. 1998, EOSTr, 79, 579
Wessel, P., Smith, W. H. F., Scharroo, R., Luis, J., & Wobbe, F. 2013, EOSTr, 94, 409
Wilson, E. H., & Atreya, S. K. 2004, JGR, 109, E06002